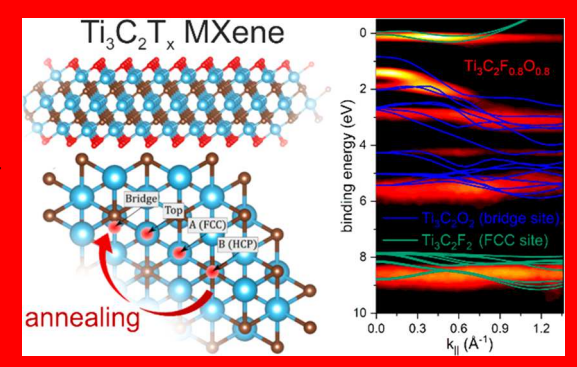


Surface Termination Dependent Work Function and Electronic Properties of Ti₃C₂T_x MXene

Thorsten Schultz, $^{\dagger,\ddagger,\parallel_{\textcircled{\tiny{0}}}}$ Nathan C. Frey, $^{\$,\parallel_{\textcircled{\tiny{0}}}}$ Kanit Hantanasirisakul, $^{\nabla,\perp,\parallel_{\textcircled{\tiny{0}}}}$ Soohyung Park, $^{\dagger,\#_{\textcircled{\tiny{0}}}}$ Steven J. May, $^{\perp}$ Vivek B. Shenoy, $^{\$}$ Yury Gogotsi, $^{\nabla,\perp_{\textcircled{\tiny{0}}}}$ and Norbert Koch*, $^{\dagger,\ddagger_{\textcircled{\tiny{0}}}}$

Supporting Information

MXenes, an emerging family of 2D transition metal carbides and nitrides, have shown promise in various applications, such as energy storage, electromagnetic interference shielding, conductive thin films, photonics, and photothermal therapy. Their metallic nature, wide range of optical absorption, and tunable surface chemistry are the key to their success in those applications. The physical properties of MXenes are known to be strongly dependent on their surface terminations. In this study, we investigated the electronic properties of Ti₃C₂T_x for different surface terminations, as achieved by different annealing temperatures, with the help of photoelectron spectroscopy, inverse photoelectron spectroscopy, and density functional theory calculations. We find that fluorine occupies solely the face-centered cubic adsorption site, whereas oxygen initially occupies at least two



different adsorption sites, followed by a rearrangement after fluorine desorption at high annealing temperatures. The measured electronic structure of Ti₃C₂T_x showed strong dispersion of more than 1 eV, which we conclude to stem from Ti-O bonds by comparing it to calculated band structures. We further measured the work function of $Ti_3C_2T_x$ as a function of annealing temperature and found that it is in the range of 3.9-4.8 eV, depending on the surface composition. A comparison of the experimental work function to detailed density functional theory calculations shows that the measured value is not simply an average of the work function values of uniformly terminated Ti₃C₂ surfaces but that the interplay between the different surface moieties and their local dipoles plays a crucial role.

INTRODUCTION

2D materials have received tremendous attention over the past decade due to their interesting properties that are different from those of their bulk counterparts, which render them promising in a variety of applications from energy storage to photonics. Typical 2D materials include graphene, transition metal dichalcogenides (TMDCs), transition metal oxides, halides and hydroxides, and hexagonal boron nitride.² Since 2011, a large family of 2D transition metal carbides and nitrides, so-called MXenes, was added to the 2D world.³ MXenes have a general formula of $M_{n+1}X_nT_x$, where M is an early transition metal such as Ti, V, Mo, and Nb, whereas X is C and/or N and Tx represents surface terminations such as OH, O, and F. MXenes are usually produced from selective etching of the A layer from MAX phases, where A is a group III to VI element, typically Al or Si. 5 Close to 30 MXenes have been produced to date, making them one of the largest and most rapidly growing families of 2D materials.⁶ Due to their metallic conductivity and versatile chemistry, they have shown promise in many applications, such as energy storage, electromagnetic interference shielding, sensors, 9,10 and photothermal therapy.¹¹ However, little is known about their fundamental electronic properties, in particular the correlation between surface termination and the MXene electronic structure. Only a handful of experiments have been reported in efforts to understand these properties, despite several theoretical calculations. 12,13 Density functional theory (DFT) studies predicted a strong influence of the surface termination type on MXenes' work function, 14 metal-to-insulator transition, 15 and electronic band occupation, 16 all of which await

Special Issue: Jean-Luc Bredas Festschrift

Received: January 28, 2019 Revised: April 3, 2019 Published: April 4, 2019



[†]Institut für Physik & IRIS Adlershof, Humboldt-Universität zu Berlin, Berlin 12489, Germany

^{*}Helmholtz-Zentrum Berlin für Materialien und Energie GmbH, Berlin 14109, Germany

[§]Department of Materials Science and Engineering, University of Pennsylvania, Philadelphia, Pennsylvania 19104, United States

VA.J. Drexel Nanomaterials Institute, Drexel University, Philadelphia, Pennsylvania 19104, United States

¹Department of Materials Science and Engineering, Drexel University, Philadelphia, Pennsylvania 19104, United States

^{*}Advanced Analysis Center, Korea Institute of Science and Technology, Seoul 02792, Korea

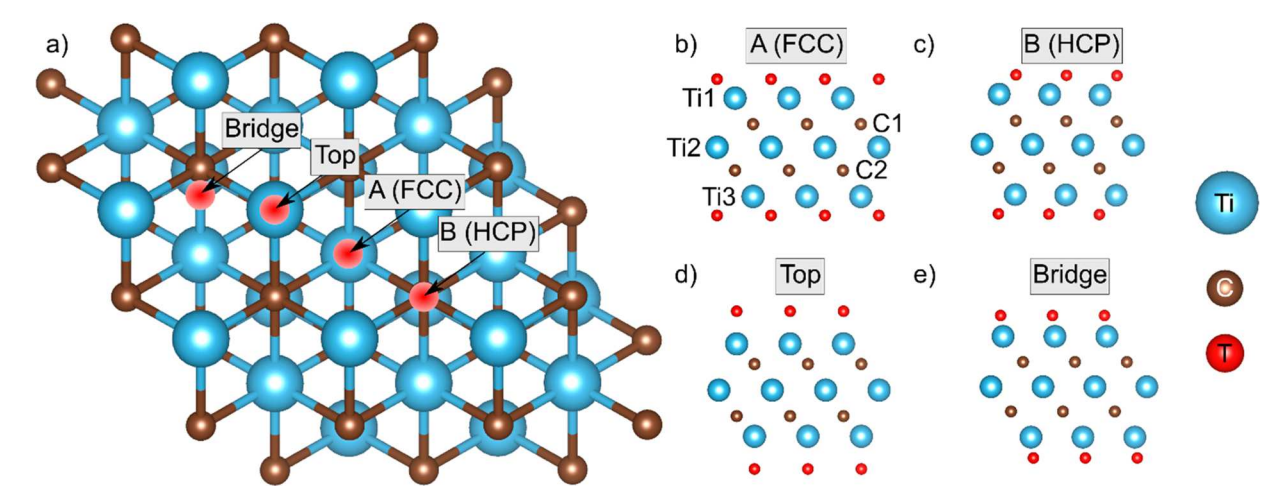


Figure 1. Schematic illustration of the different adsorption sites of $Ti_3C_2T_x$ considered for the DFT calculations in this work. (a) Top view and side views of (b) A (FCC) adsorption site (on top of Ti atom in the third atomic layer), (c) B (HCP) adsorption site (on top of C atom in the second atomic layer), (d) top adsorption site (on top of a Ti atom in the first atomic layer), and (e) bridge adsorption site (between topmost Ti and C atoms).

experimental confirmation. Reports on photoelectron spectroscopy investigations of the electronic structure of Ti₃C₂ are scarce, and only limited experimental data on the work function of this material are available. 18 In the present study, we provide direct evidence of the effects of surface termination on the work function and electronic band structure of Ti₃C₂T_r, one of the most widely studied MXenes, using a combination of ultraviolet photoemission spectroscopy (UPS), X-ray photoelectron spectroscopy (XPS), and inverse photoemission spectroscopy (IPES). By comparing our experimental results to DFT calculations, we determine the adsorption sites of the different surface terminations. This work not only provides direct experimental evidence of the effects of surface terminations on MXenes' electronic properties but also lays the groundwork for using spectroscopic techniques to study electronic properties of other MXenes. Understanding and, ultimately, being able to control their electronic properties are the key to the success in using MXenes in different applications.

METHODS

Sample Preparation. Ti₃AlC₂ (Carbon-Ukraine) was etched in a mixture of LiF and HCl following a protocol reported elsewhere. Briefly, 0.5 g of the MAX powder was added slowly to a premixed solution of 0.8 g of LiF and 10 mL of 9 M HCl. The mixture was stirred at room temperature (25 °C) for 24 h. Then, it was washed repeatedly 4 to 5 times by adding 150 mL of DI water to the mixture and centrifuged for 5 min, and the supernatant was then decanted. When the pH of the solution was close to neutral, a dark supernatant was observed indicating delamination of MXene flakes $(d-\hat{T}i_3C_2T_x)$. The first dark supernatant was decanted, and 25 mL of DI water was added to the sediment. The mixture was shaken vigorously for 15 min to improve delamination yield. Finally, the mixture was centrifuged at 3500 rpm for 30 min to collect d-Ti₃C₂T_x in the supernatant. MXene thin films were prepared by spin-casting using a spin-coater (Laurell Technologies, Model WS-650 Hz, USA). Approximately 0.5 mL of d-Ti₃C₂T_x solution with a concentration of 10 mg/mL was applied to a plasma-treated quartz substrate and spun at 2000 rpm for 30 s. The films were subsequently dried at 5000 rpm for 15 s, and the process was repeated two times to obtain films with an appropriate thickness.

Photoelectron Spectroscopy and Inverse Photoelectron Spectroscopy. Photoelectron spectroscopy measurements were performed at Humboldt University of Berlin, using two combined preparation and analysis chambers with base pressures of less than

10⁻⁸ mbar. XPS spectra were recorded using the radiation of a Mg source (1253.6 eV), and UPS spectra were recorded using the radiation of a He discharge lamp (21.21 eV). The kinetic energy of the emitted electrons was detected by a Specs Phoibos 100 hemispherical analyzer with a resolution of ≈150 meV and an angular acceptance angle of $\pm 3^{\circ}$ in the UPS measurements. During the measurements of the secondary electron cutoff, a bias of -10 V was applied between the sample and the analyzer. The XPS spectra were fitted with CasaXPS, using a Shirley-background, asymmetric line shape for peaks stemming from the MXene (due to the interaction of the photoelectrons with delocalized electrons) and Voigt line shapes for peaks stemming from contaminations. Inverse photoelectron spectroscopy (IPES) measurements were performed in the isochromat mode, using incident electron energies of 5-15 eV and a NaCl-coated photocathode for detecting the emitted photons. The resolution of the setup was determined to be 1.3 eV. The samples were resistively heated in ultrahigh vacuum inside the XPS chamber during the course of the experiment, and the spectra were measured at room temperature.

Density Functional Theory. The Vienna Ab-Initio Simulation Package (VASP)²⁰ was used for all DFT calculations. Structural relaxations were performed with the Perdew-Burke-Ernzerhof (PBE)²¹ exchange-correlation functional and projector augmented wave (PAW) pseudopotentials,²² with a 520 eV plane-wave basis cutoff, a 10 \times 10 \times 1 Γ centered k-point mesh, and forces on each atom converged to within 10^{-2} eV/Å. We assumed nonspin-polarized ground states, following previous predictions of nonmagnetic functionalized ${\rm Ti}_3{\rm C}_2{\rm T_x}^{23,24}$ To compute accurate band structures, the Heyd-Scuseria-Ernzerhof (HSE06) hybrid functional was Due to the significant computational cost of hybrid functional calculations, a $7 \times 7 \times 1 \Gamma$ centered k-point mesh was used for the HSE06 starting point, and work functions and other electronic properties were calculated for supercells using the SCAN meta-GGA functional after appropriately reducing the k-point mesh to preserve the k-point density. The core level binding energy shifts are estimated from DFT in the initial state approximation. Because the calculated absolute energies are not relevant for comparison with the experiment, only relative energy shifts are reported. The density of states (DOS) obtained from DFT were broadened with a Gaussian function with a full width at half-maximum (FWHM) of 0.4 and 1.0 eV for comparison with UPS and IPES data, respectively.

Temperature-Programmed Desorption. Thermogravimetric analysis and mass spectroscopy were performed using a Discovery SDT 650 model connected to a Discovery mass spectrometer (TA Instruments, DE). The MXene free-standing "paper" was made from the same MXene solution used in thin film fabrication via a vacuum-

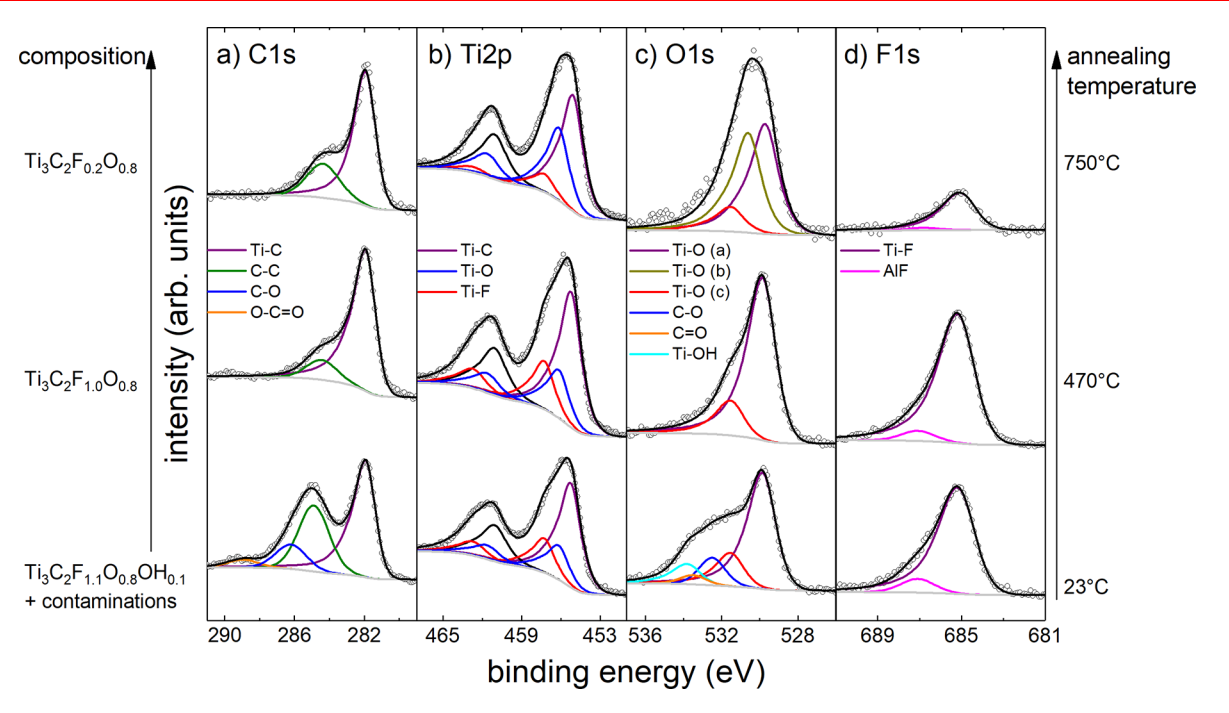


Figure 2. XPS core level spectra (a) C 1s, (b) Ti 2p, (c) O 1s, and (d) F 1s of $Ti_3C_2T_{sv}$ obtained for a sample as-loaded (lower row), after annealing at 470 °C (middle row), and after annealing at 750 °C (upper row). Hollow circles represent measured data points, and solid lines represent curve fits. The estimated surface terminations are shown on the left.

assisted filtration method. The MXene paper with a mass of ≈ 10 mg was dried in a vacuum desiccator at least 24 h prior to the measurement. Then it was packed in a 90 μ L alumina pan and heated to 1500 °C at a constant heating rate of 10 °C/min in He atmosphere (100 mL/min). The furnace was purged with a 100 mL/min flow of He gas for 1 h before the analysis to remove residual air.

Dynamic Light Scattering. Delaminated $\mathrm{Ti_3C_2T_x}$ solution with a concentration of around 0.01 mg/mL was analyzed using a Zetasizer Nano ZS (Malvern Panalytical) in a polystyrene cuvette. The average particle size was taken over a total of three measurements from each sample.

Atomic Force Microscopy. Atomic force microscopy (AFM) images were recorded with a Bruker AFM Multimode 8 in tapping mode using a driving frequency of 300 kHz, driving amplitude of 80 mV, and scanning frequency between 0.6 and 0.9 Hz.

■ RESULTS AND DISCUSSION

To identify the adsorption site of the different surface terminations and the resulting impact on the electronic structure, XPS, UPS, and IPES measurements of Ti₃C₂T_x annealed at different temperatures were compared together with DFT calculations. Figure 1 shows the different adsorption sites for surface terminations considered in this work. Figure 1a illustrates a top view of the Ti₃C₂ lattice, with the different adsorption sites marked in red, while Figure 1b-e shows the side view of the different adsorption sites. The A (FCC) site shown in Figure 1b marks the surface termination adsorbed directly above the Ti atoms in the third atomic layer (Ti2). The B (HCP) site shown in Figure 1c marks the surface termination adsorbed directly above the carbon atoms in the second atomic layer (C1). The top site shown in Figure 1d marks the surface terminations adsorbed directly above the Ti atoms in the first atomic layer (Ti1), and the bridge site shown in Figure 1e marks the surface terminations adsorbed between the topmost Ti and C atoms. These labels will be used throughout this report.

The temperature dependent XPS measurements reveal clear changes in the O 1s and C 1s core level spectra between room temperature and 470 °C, accompanied by a sharpening of the valence band as observed in UPS valence spectra. Above 500 °C, desorption of fluorine is observed, which goes hand in hand with an intensity redistribution in the O 1s core level. An overview of the XPS core level and UPS valence band evolution for different annealing temperatures is shown in Figure S1. Detailed XPS spectra of the C 1s, Ti 2p, O 1s, and F 1s core levels for three representative annealing temperatures (as loaded, 470 °C, and 750 °C) are shown in Figure 2. The C 1s core level (Figure 2a) of the as-loaded $Ti_3C_2T_x$ consists of four components. One from the Ti-C bonds of the MXene (purple) at 281.9 eV, one from C–C contaminations (green) at around 284.9 eV, and two stemming from C-O (blue) and O-C=O (orange) contaminations at 286.2 and 288.9 eV, respectively. With increasing annealing temperature, the contaminations desorb. At 470 °C, the C-O and O-C=O contaminations are completely removed, only C-C contaminations remain up to 750 °C, in agreement with previous reports. 29,30 The Ti 2p peaks shown in Figure 2b consist of three doublets (spin-orbit splitting). The doublet at 455.2 and 461.1 eV (purple) stems from Ti-C bonds of the MXene; the doublet at 456.2 and 461.6 eV stems from Ti-O (blue), and the doublet at 457.3 and 462.7 eV stems from Ti-F (red), respectively. The absence of a peak at around 459 eV indicates that no TiO2 has formed during the sample preparation or the annealing process. 31,32 No significant change in the Ti 2p spectra is observed for all annealing temperatures. Figure 2c shows the O 1s spectra, where we observe that the spectra for the as-loaded sample consists of at least five peaks, of which the peaks at 529.8 eV (purple) and 531.6 eV (red) are assigned to oxygen bound to titanium at different lattice sites. Calculation of the relative binding energy shifts by DFT (Table S1) suggests that the peak at 529.8 eV stems from oxygen on a bridge site and the peak at 531.6 eV is due to either oxygen on

the B site or oxygen on the A site in the presence of fluorine, as suggested by Persson et al.²⁹ However, considering the relative formation energies for the different adsorption sites (Table S2), only oxygen on the top adsorption site can be confidently excluded. The blue peak at 532.5 eV is assigned to C-O contaminations and the orange peak at 533.4 eV is assigned to C=O contaminations, in agreement with the C 1s core level signal. The light blue peak at 533.8 eV could be due to adsorbed water or OH surface termination groups.³³ Similar to the C 1s core level, the C-O and C=O contaminations as well as the OH terminations are completely removed after annealing at 470 °C. This is in good agreement with observations from temperature-programmed desorption measurements (Figure S2). After annealing at 750 °C, the O 1s peak becomes broader and can only be fitted adequately by adding a third peak at 530.7 eV (dark yellow). The F 1s core level shown in Figure 2d consists of one peak assigned to Ti-F surface termination (purple) at 685.2 eV and a small peak at 687.1 eV, which can be assigned to F-containing contaminations from the etching of the MAX phase. 34,35 The fluorine starts to desorb above 500 °C and is reduced by about 60-80 at. % at 750 °C, which is simultaneous with the emergence of the new peak in the O 1s spectrum. Persson et al. assigned this peak to oxygen on the A site in the absence of surrounding fluorine,²⁹ in agreement with our calculated relative binding energy shifts. From the survey spectra (Figure S3), it can be observed that a very small amount of Cl (<2%), from the LiF + HCl etchant, is present at all temperatures.

We now discuss the electronic structure of $Ti_3C_2T_r$ as inferred from UPS. The valence band spectrum of as-loaded $Ti_3C_2T_x$ (Figure S1) is dominated by carbon contaminations and does not show many features. After desorption of the contaminations, the valence band becomes sharper and shows a distinct Fermi-edge, which is a clear indication for the metallic character of the Ti₃C₂T_x. Features around 2, 3.5, 6, and 9 eV binding energy are also observed. The valence band spectra, after background subtraction and normalization (see Figure S4 for details), are shown in Figure 3a for two different surface terminations ($Ti_3C_2F_{0.8}O_{0.8}$, solid lines; $Ti_3C_2F_{0.2}O_{0.8}$, dashed lines). After annealing at 750 °C, a strong decrease of the fluorine F 1s signal was observed in XPS (see Figure 2d), which goes along with a decrease of the valence band peak at around 9 eV as well as the peak close to the Fermi-level (set to 0 eV binding energy). Therefore, we assign these two features to DOS associated with fluorine surface termination. A comparison to the calculated total DOS of Ti₃C₂F₂ shown in Figure 3b, as well as the single XPS peak in the F 1s core level (Figure 2d), clearly identifies the fluorine to be solely adsorbed on the A site. This is in agreement with findings by Persson et al.²⁹ However, a clear assignment of the oxygen adsorption site cannot be made from a comparison between the measured valence band and the calculated density of states of Ti₃C₂O₂ shown in Figure 3c, as the total DOS for the A, B, and bridge sites are very similar. Only the top adsorption site can be ruled out, as the intensity around 6 eV, which stems from oxygen termination, is not present in the total DOS for the top site. This agrees with the high formation energy of this adsorption site, as mentioned before. It should be mentioned at this point that a direct comparison between measured UPS spectra and calculated DOS from DFT must be interpreted with care, as the Kohn-Sham approximation applied in DFT neglects many body effects.

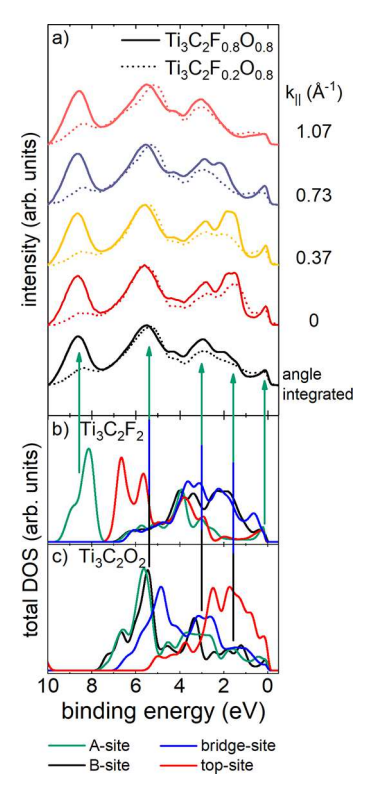


Figure 3. (a) UPS valence band spectra of ${\rm Ti}_3C_2F_{0.8}O_{0.8}$ (solid lines) and ${\rm Ti}_3C_2F_{0.2}O_{0.8}$ (dashed lines) for different k_\parallel values and angle integrated. Dispersion can be observed between 1 and 3 eV binding energy. (b, c) The calculated total DOS for ${\rm Ti}_3C_2F_2$ and ${\rm Ti}_3C_2O_2$ terminations at different adsorption sites. Arrows indicate the correlations between calculations and experimental data.

Figure 3a shows additional UPS spectra for different photoelectron momentum values parallel to the sample surface $(k_{\parallel}, \text{ corresponding to different takeoff angles})$. There is an obvious angular dependence in the features between 1.5 and 3 eV, which is an indication for band dispersion. Normally, the observation of band dispersion is only expected for single crystalline samples. However, there have been examples of nonsingle crystalline graphite and transition metal dichalcogenides (TMDCs), which showed dispersive bands in angleresolved photoemission measurements (ARPES).36,37 The high symmetry of the crystal lattice and the particular azimuthal photoemission-intensity dependence enable a measurement of the dispersion, which is dominated by the high-symmetry directions (Γ -M and Γ -K; for a more detailed explanation, see Figure S5). A curvature plot, as obtained from the measured ARPES data by following a procedure described by Zhang et al., ³⁸ for a Ti₃C₂F_{0.8}O_{0.8} sample is shown in Figure 4a. Nondispersive bands are visible around 5.5 and 9 eV, corresponding to oxygen and fluorine surface terminations, respectively, as discussed earlier. Notably, rather dispersive bands can be seen from about 1.5 eV binding energy to about 3 eV binding energy, when moving from $k_{\parallel} = 0 \text{ Å}^{-1}$ to $k_{\parallel} = 1.2$ Å-1. Selected bands from the calculated band structure of $Ti_3C_2F_2$ with fluorine adsorbed at the A site as well as $Ti_3C_2O_2$ with oxygen adsorbed at the bridge site are included in Figure 4a for comparison, and the complete band calculations are presented in Figure 4b. The calculated bands for the Ti₃C₂F₂ termination are in good agreement with the nondispersive feature around 9 eV and with the dispersive feature around the Fermi-level. The calculated bands for oxygen adsorbed at the

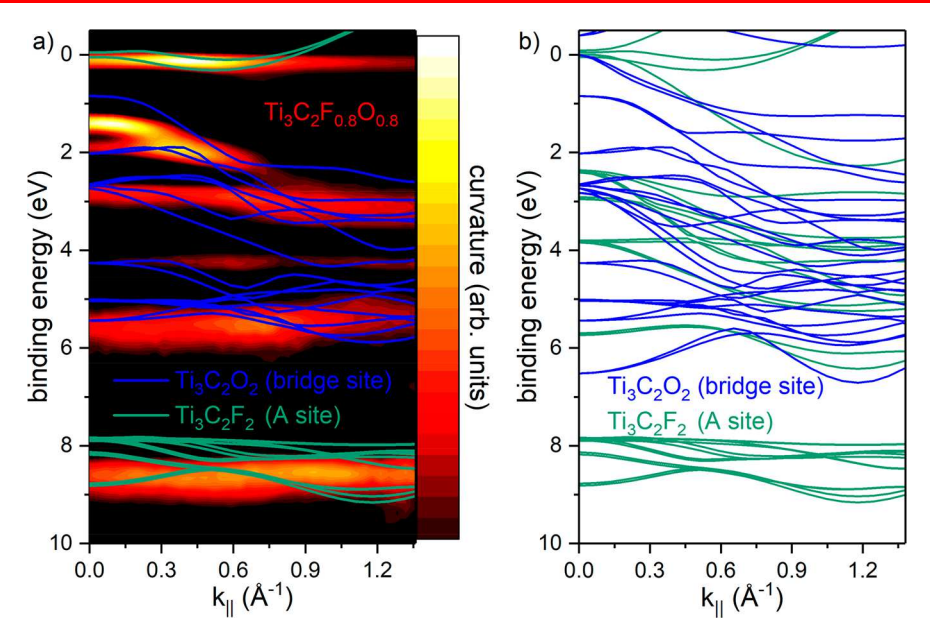


Figure 4. (a) Measured ARPES curvature spectrum of $Ti_3C_2F_{0.8}O_{0.8}$ (yellow-red), including a selected part of the calculated band structures of the high-symmetry Γ -K and Γ -M directions for $Ti_3C_2O_2$ with O adsorbed only on the bridge site (blue) and for $Ti_3C_2F_2$ with F adsorbed only on the A site (green). (b) Full calculated band structures of the high-symmetry Γ -K and Γ -M directions for $Ti_3C_2O_2$ with O adsorbed only on the bridge site (blue) and for $Ti_3C_2F_2$ with F adsorbed only on the A site (green). The DFT calculations were done using the range-separated hybrid HSE06 functional and predicted more bands than are observed in the curvature plot of the experimental data.

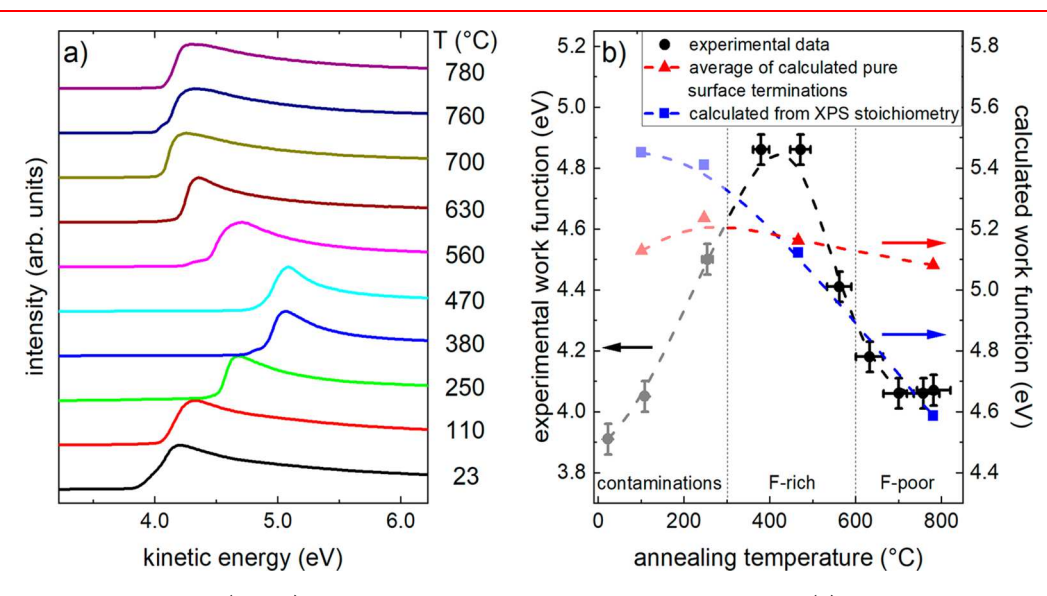


Figure 5. (a) Secondary electron cutoff (SECO) spectra of $Ti_3C_2T_x$ annealed at different temperatures. (b) Work function values determined from the SECOs in (a) as a function of annealing temperature. Work functions obtained from DFT for different surface terminations, calculated by using the real surface stoichiometry obtained from XPS (blue) and obtained by averaging the work functions of purely terminated $Ti_3C_2O_2$, $Ti_3C_2F_2$, $Ti_3C_2OH_2$, and Ti_3C_2 surfaces, weighted by the experimentally determined stoichiometry (red).

bridge site agree fairly well with the nondispersive feature at around 5.5 eV and with the dispersive features between 1.5 and 3 eV. All other calculated band structures derived from different adsorption sites of the surface terminations are shown in Figure S6, showing less agreement with the measured ARPES spectrum. However, the O1s XPS core level spectra (Figure 2c) consist of at least two peaks after removal of surface terminations, and a third peak emerges after desorption of fluorine (dark yellow peak in Figure 2c). This new peak can be related to oxygen at the A site in the absence of surrounding fluorine. This is also in agreement with findings by Persson et al.²⁹ Therefore, it is not surprising that the band structure

calculated using only a single termination site cannot capture all the features observed in the ARPES measurements.

We also performed IPES measurements on the $Ti_3C_2F_{0.8}O_{0.8}$ and the $Ti_3C_2F_{0.2}O_{0.8}$ samples to probe the unoccupied states, complementing the XPS and UPS measurements of the occupied states. The IPES spectra are shown in Figure S7, together with the calculated total DOS. The IPES spectrum of the $Ti_3C_2F_{0.8}O_{0.8}$ sample shows one peak at ca. 1.9 eV binding energy, which decreases in intensity after fluorine desorption, as clearly observed when plotting the difference between the two spectra (gray). The comparison to the calculated DOS shown in Figure S7b,c suggests that this peak is in accordance

with F adsorbed on the A site, fully in line with the results obtained from XPS and UPS.

Knowing the surface composition and the most probable adsorption sites, we can now attend to the evolution of the $Ti_3C_2T_r$ work function for different surface terminations, as the exact composition and adsorption site influence the calculated work function obtained from DFT. The work function of the Ti₃C₂T_{xt} as determined from the secondary electron cut-offs (SECOs, shown in Figure 5a), is summarized in Figure 5b as a function of annealing temperature (for exact composition at each temperature, see Figure S8). The as-loaded Ti₃C₂T_x exhibits relatively low work function of ca. 3.9 eV, which increases to 4.8 eV after annealing at 380 °C. One possible explanation could be a desorption of residual contaminations, like LiF or Al from the sample preparation process, or atmospheric water, carbon, or carbon oxides, which are known to decrease the work function of clean metals via the push-back effect.^{39,40} Another reason could be the desorption of OH surface terminations, which are predicted to significantly decrease the work function of Ti₃C₂. 14,41 Due to the low amount of OH groups as suggested by XPS results, the former is more likely. The maximum work function of 4.8 eV is significantly lower than the predicted work function of Ti₃C₂O₂ (≈6 eV) but significantly higher than the predicted work function of bare Ti₃C₂ (3.9 eV).⁴¹ With desorption of fluorine at higher temperatures, the work function decreases again and saturates at ca. 4.1 eV. Work function values obtained from DFT calculations are also shown in Figure 5b. The red dots show an averaged work function, obtained by weighting the work function values of the homogeneously terminated surfaces (Ti₃C₂O₂, Ti₃C₂F₂, Ti₃C₂OH₂, and Ti₃C₂) with the fraction of the different terminations obtained by evaluating the XPS core level peaks for the different annealing temperatures (Figure S8). As can be seen, simply averaging the work function of the purely terminated surfaces does not sufficiently resemble the measured work function. A more involved procedure to calculate the work function was employed by constructing minimal supercells that accommodate the approximate surface stoichiometry measured by XPS and randomly distributing these terminations (see Table S3 for used surface terminations and supercell dimensions). This method more reliably accounts for the actual change in interlayer separation and local dipole distributions, resulting in a more accurate calculation of the overall surface dipole and work function. The results are shown in blue in Figure 5b. This approach leads to a significant reduction of the work function with reduced fluorine termination, in qualitative agreement with observations from the experiment at higher annealing temperatures. Deviations between the experiment and theory, especially at low annealing temperatures, stem most likely from contaminations, which cannot be included in the calculations. Additionally, we only considered randomly distributed surface terminations in our work function calculations, neglecting the possibility of reorganization of surface terminations after thermal annealing. This leaves a more detailed investigation on the behavior of the surface terminations upon annealing as a future study.

CONCLUSIONS

Through comparison of XPS, angle-resolved UPS, and IPES measurements of ${\rm Ti_3C_2T_x}$ after different annealing temperatures with DFT calculations, we identified the adsorption sites of the surface terminations. Fluorine occupies the face-

centered cubic adsorption site, and oxygen initially occupies the bridge site and the hexagonal close-packed site, followed by a rearrangement to the face-centered cubic site after fluorine desorption at high annealing temperatures. Good agreement was found between calculated band structures for these adsorption sites and ARPES measurements, showing dispersion of more than 1 eV. Upon heating in vacuum, the sample work function increases from 3.9 to 4.8 eV, most probably due to desorption of water, carbon-dominated contaminations, and OH species, and decreases again at higher temperatures to 4.1 eV due to fluorine desorption. We find that the measured work function cannot be obtained by simply averaging the work function values of purely terminated Ti₂C₂T_r surfaces, but it can be better reproduced by modeling the real surface mixed termination to account for local dipole effects. Our findings represent a solid foundation for the possibilities of determining the composition and electronic properties of MXenes with photoemission spectroscopy and will help to further explore and understand this new class of 2D materials.

ASSOCIATED CONTENT

Supporting Information

The Supporting Information is available free of charge on the ACS Publications website at DOI: 10.1021/acs.chemmater.9b00414.

Calculated binding energies for different oxygen adsorption sites; calculated lattice parameters and formation energies for different surface terminations on different adsorption sites; surface terminations and supercell dimensions used for work function calculations; core level and valence spectra for different annealing temperatures; temperature-programmed desorption measurement; XPS survey spectra; UPS background subtraction procedure; Brillouin zone schematic and explanations for observation of band dispersion mainly along the high-symmetry directions; calculated band structures for different surface terminations and adsorption sites; IPES spectra; summary surface terminations from XPS; AFM image; dynamic light scattering measurement (PDF)

AUTHOR INFORMATION

Corresponding Author

*E-mail: nkoch@physik.hu-berlin.de.

Norbert Koch: 0000-0002-6042-6447

ORCID (

Thorsten Schultz: 0000-0002-0344-6302 Nathan C. Frey: 0000-0001-5291-6131 Kanit Hantanasirisakul: 0000-0002-4890-1444 Soohyung Park: 0000-0002-6589-7045 Yury Gogotsi: 0000-0001-9423-4032

Author Contributions

T.S., N.C.F., and K.H. contributed equally to this work.

Notes

The authors declare no competing financial interest.

ACKNOWLEDGMENTS

The work in Berlin was supported by the Deutsche Forschungsgemeinschaft (DFG), Project No. 182087777-SFB 951. N.C.F. was supported by the Department of Defense

(DoD) through the National Defense Science & Engineering Graduate Fellowship (NDSEG) Program. V.B.S. acknowledges support from the Army Research Office, contract W911NF-16-1-0447, and also grants EFMA-542879 and CMMI-1727717 from the U.S. National Science Foundation. K.H., S.J.M., and Y.G. acknowledge support for research on synthesis and electronic properties of MXenes from the U.S. Department of Energy (DOE), Office of Science, Office of Basic Energy Sciences, grant #DE-SC0018618.

REFERENCES

- (1) Novoselov, K. S.; Jiang, D.; Schedin, F.; Booth, T. J.; Khotkevich, V. V.; Morozov, S. V.; Geim, A. K. Two-dimensional atomic crystals. *Proc. Natl. Acad. Sci. U. S. A.* **2005**, *102*, 10451–10453.
- (2) Nicolosi, V.; Chhowalla, M.; Kanatzidis, M. G.; Strano, M. S.; Coleman, J. N. Liquid Exfoliation of Layered Materials. *Science* **2013**, 340, 1226419.
- (3) Naguib, M.; Kurtoglu, M.; Presser, V.; Lu, J.; Niu, J.; Heon, M.; Hultman, L.; Gogotsi, Y.; Barsoum, M. W. Two-Dimensional Nanocrystals Produced by Exfoliation of Ti₃AlC₂. *Adv. Mater.* **2011**, 23, 4248–4253.
- (4) Barsoum, M. W. MAX Phases: Properties of Machinable Ternary Carbides and Nitrides; Wiley VCH Verlag GmbH & Co. KGaA: Weinheim, Germany, 2013.
- (5) Naguib, M.; Mashtalir, O.; Carle, J.; Presser, V.; Lu, J.; Hultman, L.; Gogotsi, Y.; Barsoum, M. W. Two-Dimensional Transition Metal Carbides. *ACS Nano* **2012**, *6*, 1322–1331.
- (6) Hantanasirisakul, K.; Gogotsi, Y. Electronic and Optical Properties of Two-Dimensional Transition Metal Carbides and Nitrides (MXenes). *Adv. Mater.* **2018**, *30*, 1804779.
- (7) Anasori, B.; Lukatskaya, M. R.; Gogotsi, Y. 2D metal carbides and nitrides (MXenes) for energy storage. *Nat. Rev. Mater.* **2017**, *2*, 16098.
- (8) Shahzad, F.; Alhabeb, M.; Hatter, C. B.; Anasori, B.; Man Hong, S.; Koo, C. M.; Gogotsi, Y. Electromagnetic interference shielding with 2D transition metal carbides (MXenes). *Science* **2016**, 353, 1137–1140.
- (9) Kim, S. J.; Koh, H.-J.; Ren, C. E.; Kwon, O.; Maleski, K.; Cho, S.-Y.; Anasori, B.; Kim, C.-K.; Choi, Y.-K.; Kim, J.; et al. Metallic ${\rm Ti}_3{\rm C}_2{\rm T}_{\rm x}$ MXene Gas Sensors with Ultrahigh Signal-to-Noise Ratio. *ACS Nano* **2018**, *12*, 986–993.
- (10) Ma, Y.; Liu, N.; Li, L.; Hu, X.; Zou, Z.; Wang, J.; Luo, S.; Gao, Y. A highly flexible and sensitive piezoresistive sensor based on MXene with greatly changed interlayer distances. *Nat. Commun.* **2017**, *8*, 1207.
- (11) Huang, K.; Li, Z.; Lin, J.; Han, G.; Huang, P. Two-dimensional transition metal carbides and nitrides (MXenes) for biomedical applications. *Chem. Soc. Rev.* **2018**, *47*, 5109–5124.
- (12) Römer, F. M.; Wiedwald, U.; Strusch, T.; Halim, J.; Mayerberger, E.; Barsoum, M. W.; Farle, M. Controlling the conductivity of Ti₃C₂ MXenes by inductively coupled oxygen and hydrogen plasma treatment and humidity. *RSC Adv.* **2017**, *7*, 13097–13103
- (13) Hart, J. L.; Hantanasirisakul, K.; Lang, A. C.; Anasori, B.; Pinto, D.; Pivak, Y.; van Omme, J. T.; May, S. J.; Gogotsi, Y.; Taheri, M. L. Control of MXenes' Electronic Properties Through Termination and Intercalation. *Nat. Commun.* **2019**, *10*, 522.
- (14) Khazaei, M.; Arai, M.; Sasaki, T.; Ranjbar, A.; Liang, Y.; Yunoki, S. OH-terminated two-dimensional transition metal carbides and nitrides as ultralow work function materials. *Phys. Rev. B: Condens. Matter Mater. Phys.* **2015**, *92*, 075411.
- (15) Khazaei, M.; Arai, M.; Sasaki, T.; Chung, C.-Y.; Venkataramanan, N. S.; Estili, M.; Sakka, Y.; Kawazoe, Y. Novel Electronic and Magnetic Properties of Two-Dimensional Transition Metal Carbides and Nitrides. *Adv. Funct. Mater.* **2013**, *23*, 2185–2192.

(16) Khazaei, M.; Ranjbar, A.; Arai, M.; Sasaki, T.; Yunoki, S. Electronic properties and applications of MXenes: a theoretical review. *J. Mater. Chem. C* **2017**, *5*, 2488–2503.

- (17) Magnuson, M.; Halim, J.; Näslund, L.-Å. Chemical bonding in carbide MXene nanosheets. J. Electron Spectrosc. Relat. Phenom. 2018, 224, 27–32.
- (18) Wang, Z.; Kim, H.; Alshareef, H. N. Oxide Thin-Film Electronics using All-MXene Electrical Contacts. *Adv. Mater.* **2018**, 30, 1706656.
- (19) Alhabeb, M.; Maleski, K.; Anasori, B.; Lelyukh, P.; Clark, L.; Sin, S.; Gogotsi, Y. Guidelines for Synthesis and Processing of Two-Dimensional Titanium Carbide (Ti₃C₂T_x MXene). *Chem. Mater.* **2017**, 29, 7633–7644.
- (20) Kresse, G.; Furthmüller, J. Efficient iterative schemes for ab initio total-energy calculations using a plane-wave basis set. *Phys. Rev. B: Condens. Matter Mater. Phys.* **1996**, *54*, 11169–11186.
- (21) Perdew, J. P.; Burke, K.; Ernzerhof, M. Generalized Gradient Approximation Made Simple. *Phys. Rev. Lett.* **1996**, *77*, 3865–3868.
- (22) Kresse, G.; Joubert, D. From ultrasoft pseudopotentials to the projector augmented-wave method. *Phys. Rev. B: Condens. Matter Mater. Phys.* **1999**, *59*, 1758–1775.
- (23) Xie, Y.; Naguib, M.; Mochalin, V. N.; Barsoum, M. W.; Gogotsi, Y.; Yu, X.; Nam, K.-W.; Yang, X.-Q.; Kolesnikov, A. I.; Kent, P. R. C. Role of Surface Structure on Li-Ion Energy Storage Capacity of Two-Dimensional Transition-Metal Carbides. *J. Am. Chem. Soc.* **2014**, *136*, 6385–6394.
- (24) Wu, F.; Luo, K.; Huang, C.; Wu, W.; Meng, P.; Liu, Y.; Kan, E. Theoretical understanding of magnetic and electronic structures of ${\rm Ti}_3{\rm C}_2$ monolayer and its derivatives. *Solid State Commun.* **2015**, 222, 9–13.
- (25) Heyd, J.; Scuseria, G. E.; Ernzerhof, M. Hybrid functionals based on a screened Coulomb potential. *J. Chem. Phys.* **2003**, *118*, 8207–8215.
- (26) Krukau, A. V.; Vydrov, O. A.; Izmaylov, A. F.; Scuseria, G. E. Influence of the exchange screening parameter on the performance of screened hybrid functionals. *J. Chem. Phys.* **2006**, *125*, 224106.
- (27) Sun, J.; Ruzsinszky, A.; Perdew, J. P. Strongly Constrained and Appropriately Normed Semilocal Density Functional. *Phys. Rev. Lett.* **2015**, *115*, 036402.
- (28) Zhang, Y.; Sun, J.; Perdew, J. P.; Wu, X. Comparative first-principles studies of prototypical ferroelectric materials by LDA, GGA, and SCAN meta-GGA. *Phys. Rev. B: Condens. Matter Mater. Phys.* **2017**, *96*, 035143.
- (29) Persson, I.; Näslund, L.-Å.; Halim, J.; Barsoum, M. W.; Darakchieva, V.; Palisaitis, J.; Rosen, J.; Persson, P.O.Å. On the organization and thermal behavior of functional groups on Ti₃C₂ MXene surfaces in vacuum. 2D Mater. 2018, 5, 015002.
- (30) Kong, F.; He, X.; Liu, Q.; Qi, X.; Zheng, Y.; Wang, R.; Bai, Y. Improving the electrochemical properties of MXene Ti₃C₂ multilayer for Li-ion batteries by vacuum calcination. *Electrochim. Acta* **2018**, 265, 140–150.
- (31) Diebold, U.; Madey, T. E. ${\rm TiO_2}$ by XPS. Surf. Sci. Spectra 1996, 4, 227–231.
- (32) Kurtz, R. L.; Henrich, V. E. Comparison of Ti 2p Core-Level Peaks from TiO₂, Ti₂O₃, and Ti Metal, by XPS. *Surf. Sci. Spectra* **1998**, 5, 179–181.
- (33) Shen, C.; Wang, L.; Zhou, A.; Wang, B.; Wang, X.; Lian, W.; Hu, Q.; Qin, G.; Liu, X. Synthesis and Electrochemical Properties of Two-Dimensional RGO/ ${\rm Ti}_3{\rm C}_2{\rm T}_{\rm x}$ Nanocomposites. *Nanomaterials* **2018**, *8*, 80.
- (34) Shah, S. A.; Habib, T.; Gao, H.; Gao, P.; Sun, W.; Green, M. J.; Radovic, M. Template-free 3D titanium carbide $(Ti_3C_2T_x)$ MXene particles crumpled by capillary forces. *Chem. Commun.* **2017**, *53*, 400–403
- (35) Cao, Y.; Deng, Q.; Liu, Z.; Shen, D.; Wang, T.; Huang, Q.; Du, S.; Jiang, N.; Lin, C.-T.; Yu, J. Enhanced thermal properties of poly(vinylidene fluoride) composites with ultrathin nanosheets of MXene. *RSC Adv.* **2017**, *7*, 20494–20501.

(36) Park, S.; Mutz, N.; Schultz, T.; Blumstengel, S.; Han, A.; Aljarb, A.; Li, L.-J.; List-Kratochvil, E. J. W.; Amsalem, P.; Koch, N. Direct determination of monolayer MoS₂ and WSe₂ exciton binding energies on insulating and metallic substrates. 2D Mater. **2018**, 5, 025003.

- (37) Zhou, S. Y.; Gweon, G.-H.; Spataru, C. D.; Graf, J.; Lee, D.-H.; Louie, S. G.; Lanzara, A. Coexistence of sharp quasiparticle dispersions and disorder features in graphite. *Phys. Rev. B: Condens. Matter Mater. Phys.* **2005**, *71*, 161403.
- (38) Zhang, P.; Richard, P.; Qian, T.; Xu, Y.-M.; Dai, X.; Ding, H. A precise method for visualizing dispersive features in image plots. *Rev. Sci. Instrum.* **2011**, *82*, 043712.
- (39) Heras, J. M.; Viscido, L. Work function changes upon water contamination of metal surfaces. *Appl. Surf. Sci.* **1980**, *4*, 238–241.
- (40) Helander, M. G.; Greiner, M. T.; Wang, Z. B.; Lu, Z. H. Pitfalls in measuring work function using photoelectron spectroscopy. *Appl. Surf. Sci.* **2010**, *256*, 2602–2605.
- (41) Caffrey, N. M. Effect of mixed surface terminations on the structural and electrochemical properties of two-dimensional ${\rm Ti_3C_2T_2}$ and ${\rm V_2CT_2}$ MXenes multilayers. Nanoscale **2018**, 10, 13520–13530.